Biosensors and Bioelectronics 86 (2016) 756–763

Contents lists available at ScienceDirect

Biosensors and Bioelectronics

journal homepage: www.elsevier.com/locate/bios

# Paper analytical devices for dynamic evaluation of cell surface N-glycan expression via a bimodal biosensor based on multibranched hybridization chain reaction amplification

Linlin Liang [a], Feifei Lan [a], Li Li [a], Shenguang Ge [a,b,*], Jinghua Yu [a], Na Ren [c], Haiyun Liu [a], Mei Yan [a]

[a] School of Chemistry and Chemical Engineering, University of Jinan, Jinan, 250022 China
[b] Shandong Provincial Key Laboratory of Preparation and Measurement of Building Materials, University of Jinan,, Jinan, 250022 China
[c] School of Biological Science and Technology, University of Jinan, Jinan, 250022 China

ARTICLE INFO

*Article history:*
Received 19 May 2016
Received in revised form
10 July 2016
Accepted 22 July 2016
Available online 25 July 2016

*Keywords:*
Colorimetric/fluorescence bimodal biosensor
PtCu nanochains
Graphene quantum dot
Multibranched hybridization chain reaction
Au-Ag-paper devices

ABSTRACT

A novel colorimetric/fluorescence bimodal lab-on-paper cyto-device was fabricated based on concanavalin A (Con A)-integrating multibranched hybridization chain reaction (mHCR). The product of mHCR was modified PtCu nanochains (colorimetric signal label) and graphene quantum dot (fluorescence signal label) for in situ and dynamically evaluating cell surface N-glycan expression. In this strategy, preliminary detection was carried out through colorimetric method, if needed, then the fluorescence method was applied for a precise determination. Au-Ag-paper devices increased the surface areas and active sites for immobilizing larger amount of aptamers, and then specifically and efficiently captured more cancer cells. Moreover, it could effectively reduce the paper background fluorescence. Due to the specific recognition of Con A with mannose and the effective signal amplification of mHCR, the proposed strategy exhibited excellent high sensitivity for the cytosensing of MCF-7 cells ranging from 100 to $1.0 \times 10^7$ and 80-$5.0 \times 10^7$ cells $mL^{-1}$ with the detection limit of 33 and 26 cells $mL^{-1}$ for colorimetric and fluorescence, respectively. More importantly, this strategy was successfully applied to dynamically monitor cell-surface multi-glycans expression on living cells under external stimuli of inhibitors as well as for N-glycan expression inhibitor screening. These results implied that this biosensor has potential in studying complex native glycan-related biological processes and elucidating the N-glycan-related diseases in biological and physiological processes.



## 1. Introduction

Cells are covered by a large number of glycans which are covalently attached to underlying proteins or lipids with high density and complex diversity (Pilobello et al., 2007). The carbohydrate on the surface of a eukaryotic cell is in a complex milieu and plays vital roles in a broad range of crucial biological and physiological processes, including growth, development, differentiation, cell adhesion, cell-cell communication, signaling, immune response, disease, and progression of cancer (Dennis et al., 2009; Gu et al., 2012). As a result, glycan epitopes are generally the surface markers to detect the different expression during a variety of cell biological processes (Arnold et al., 2011). It is critical both to understand their role in disease development as well as to provide effective diagnostic tools to help guide cancer therapeutics. Currently, various approaches, including high-performance liquid chromatography (Royle et al., 2008), mass spectrometry (Nishikaze et al., 2012), nuclear magnetic resonance (Carneiro et al., 2015), and capillary electrophoresis (Vanderschaeghe et al., 2010), have been applied for glycan analysis. However, these methods are not feasible for the in situ and dynamically evaluating N-glycan expression of living cells due to their destructive procedures. Furthermore, these approaches are time-consuming, with complicated sample preparation and sophisticated instrumentation.

Microfluidic paper-based analytical devices (μPADs) have appeared as a very potential platform for cell culture and cell-based assays (Meyvantsson et al., 2008; Yeo et al., 2011; Kovarik et al., 2012). In particular, the μPADs typically exhibit low sample and reagent consumption, low cost, small size, portable, easy modification and operation. The great number of advantages make the μPADs play a potential platform for the facile and fast analysis of the glycan profiling in a high-throughput manner (Primack et al., 2011). In clinic, two or more detection methods are usually applied

* Corresponding author at: School of Chemistry and Chemical Engineering, University of Jinan, Jinan 250022, China.
*E-mail address:* chm_gesg@163.com (S. Ge).

http://dx.doi.org/10.1016/j.bios.2016.07.078
0956-5663/

together to reach more reliable diagnostic results, since each method has its specific advantages as well as limitations. For example, colorimetric is the most commonly method on μPADs (Li et al., 2011) because of the easy operation and straightforward signal readout, but relatively low sensitivity. The fluorescence (Deiss et al., 2013; Deiss et al., 2014; Liang et al., 2016) is another kind of optical method possessing inherently much higher sensitivity than colorimetry, While its relatively sophisticated and expensive. Thus, we combined the colorimetric and fluorescence on μPADs to achieve the determination of cells and cell surface N-glycan expression. Due to the previously discussed advantages, a dense interconnected Au-Ag nanoparticles (NPs) layer was grown on the surfaces of cellulose fibers in the paper sample zone, which were used as carriers for a large sum of tumor cells. Moreover, it could effectively reduce the paper background fluorescence signal.

To further perform high sensitivity visible colorimetric and fluorescent analysis, more attention has been paid on nanomaterials and popular strategies for signal amplification. Recently, zhu et al. have addressed green-photoluminescent graphene quantum dots for bioimaging applications (Zhu et al., 2011). As newcomers to the carbon nanomaterials family, graphene quantum dots (GQDs) (Loh et al., 2010) has attracted increasing attention, owing to their unique chemical and physical properties, such as low toxicity, easy preparation, broad excitation spectra, photobleaching resistance, a larger Stokes shift over conventional organic fluorophores (Wu et al., 2009; Gosso et al., 2011; Ratanatawanate et al., 2011; Wang et al., 2010) and narrow, symmetric, and tunable emission spectra. Because of these attractive merits, GQDs have been widely used in bioimaging, drug delivery, fluorescence sensors and optoelectronic devices. In this work, the prepared GQDs showed a relatively strong fluorescence and bright blue emission under excitation of 365 nm UV light. Recently, multicomponent nanostructures (Ge et al., 2014) have attracted tremendous attention. Their surface area, catalytic performance and biocompatibility could be enhanced by the synergistic and the electronic effects between different components. There have been several reports regarding enzymeless biosensors based on $Pt_xM_{1-x}$ alloy nanomaterials (Park et al., 2012; Ding et al., 2012). For example, Nanoporous PtCu alloys were also employed for glucose sensing (Xu et al., 2011). Compared with single metal PtNPs, the $Pt_xM_{1-x}$ alloys present distinctly synergetic characteristics, in which Pt shows the specific catalytic activity, and the other metal takes on a biocompatibility, an increasement of the active sites and the enhancement of the long-term stability. Therefore, $Pt_xM_{1-x}$ alloys provide rapid response, good stability and high catalytic efficiency. Due to the previously discussed advantages, PtCu nanochains as mimicking natural peroxidases was fabricated to assay cells using the colorimetric assay. Moreover, the multibranched hybridization chain reaction (mHCR) has not been investigated previously in the colorimetric and fluorescence cytosensing on μPADs. Different from the conventional HCR, the mHCR can produce long products with multiple branched arms (Huang et al., 2011; Choi et al., 2010; Lan et al., 2016). It could attach abundant PtCu nanochains and GQDs for efficient signal amplification, which significantly enhanced the sensitivity of the biosensors.

Therefore, in this work, we successfully designed a novel lab-on-paper cyto-device based on concanavalin A (Con A)-integrating mHCR. The product of mHCR was modified PtCu nanochains and GQDs (PtCu-mHCR-GQDs) for dynamically evaluating cell surface N-glycan expression. Compared with the previously reported fluorescence-based cell surface N-glycan expression detection strategies, our proposed method possessed some remarkable features: (1) Au-Ag-paper devices not only increased the surface areas and active sites to immobilize more cancer cells but also could effectively reduce the paper background fluorescence. (2) PtCu nanochains showed superior peroxidase-like catalytic performance. (3) The mHCR could produce long products with multiple branched arms for signal amplification (4) This biosensor combined the colorimetric and fluorescence method to visual detection of cell surface N-glycan. Therefore, the developed biosensor holds potential for ultrasensitive visual detection of cell surface N-glycan expression and supplies valuable information for diabetes mellitus research and clinical diagnosis.

## 2. Experimental section

### 2.1. Preparation of PtCu nanochains

The PtCu nanochains were synthesized according to the literature (Cao et al., 2013). The detailed preparation process for PtCu nanochains were provided in the Supplementary information.

### 2.2. Preparation of PtCu-mHCR-GQDs

The mHCR was carried out in a similar way to the reported method created by Pierce's group (Dirks et al., 2004) and a detailed procedure was described in the Supplementary information.

### 2.3. Preparation of the Ag-Au-μPADs

The fabrication of the 3D μPADs was similar to our previous work (Li et al., 2013; Ge et al., 2012) and a detailed procedure was described in the Supplementary information (Scheme S1, Figs. S1–S3). Prior to the mobilization, the novel Ag-Au-μPADs was fabricated on the surfaces of cellulose fibers in the fluorescence layer sample zone of μPADs to enlarge effectively surface area μPADs for the further immobilization of aptamer array. The fabrication procedures of the Ag-Au-μPADs were described in the Supplementary information.

### 2.4. Operation and assay procedures of this biosensor

The schematic diagram of the N-glycan biosensor format was shown in Scheme 1. MCF-7 cell-targeting aptamer was chosen as molecular probes to functionalize the Ag-Au-μPADs due to their salient properties, such as specificity and high affinity, good stability, ease of chemical modification and low immunogenicity (Bagalkot et al., 2006; Shangguan et al., 2006). Briefly, on the α-sheet, 10 μL of 4.0 μM aptamer solution was dropped into corresponding paper cell zone, and incubated at room temperature for 15 min. Then, physically absorbed excess aptamers were carefully rinsed. Subsequently, a drop of 10 μL 2% BSA solution was injected into each aptamer/Ag-Au-μPADs and allowed to react at room temperature for 5 min to ensure the blocking of nonspecific binding sites. Thereafter, 10 μL of homogeneous MCF-7 cell suspension at a certain concentration was dropped into each BSA/aptamer/Ag-Au-μPADs and incubated at room temperature for 15 min (Fig. S4A) to capture the cells though the specific binding between the immobilized aptamers and cells. Then, the obtained MCF-7/BSA/aptamer/Ag-Au-μPADs were carefully rinsed with incubation buffer to remove the noncaptured cells, and ready for subsequent assays.

The colorimetric and fluorescence detection of N-glycan could be achieved using PtCu-mHCR-GQDs. Firstly, the PtCu-mHCR-GQDs bioprobe was dropped into the prepared paper zone in the middle, and incubated for 5 min (Fig. S4B). For the binding of PtCu-mHCR-GQDs to mannose on captured MCF-7 cell membrane, 0.1 mM $Ca^{2+}$ and $Mn^{2+}$ should be added to PtCu-mHCR-GQDs solution. The fluorescence spectra were obtained on a LS-55

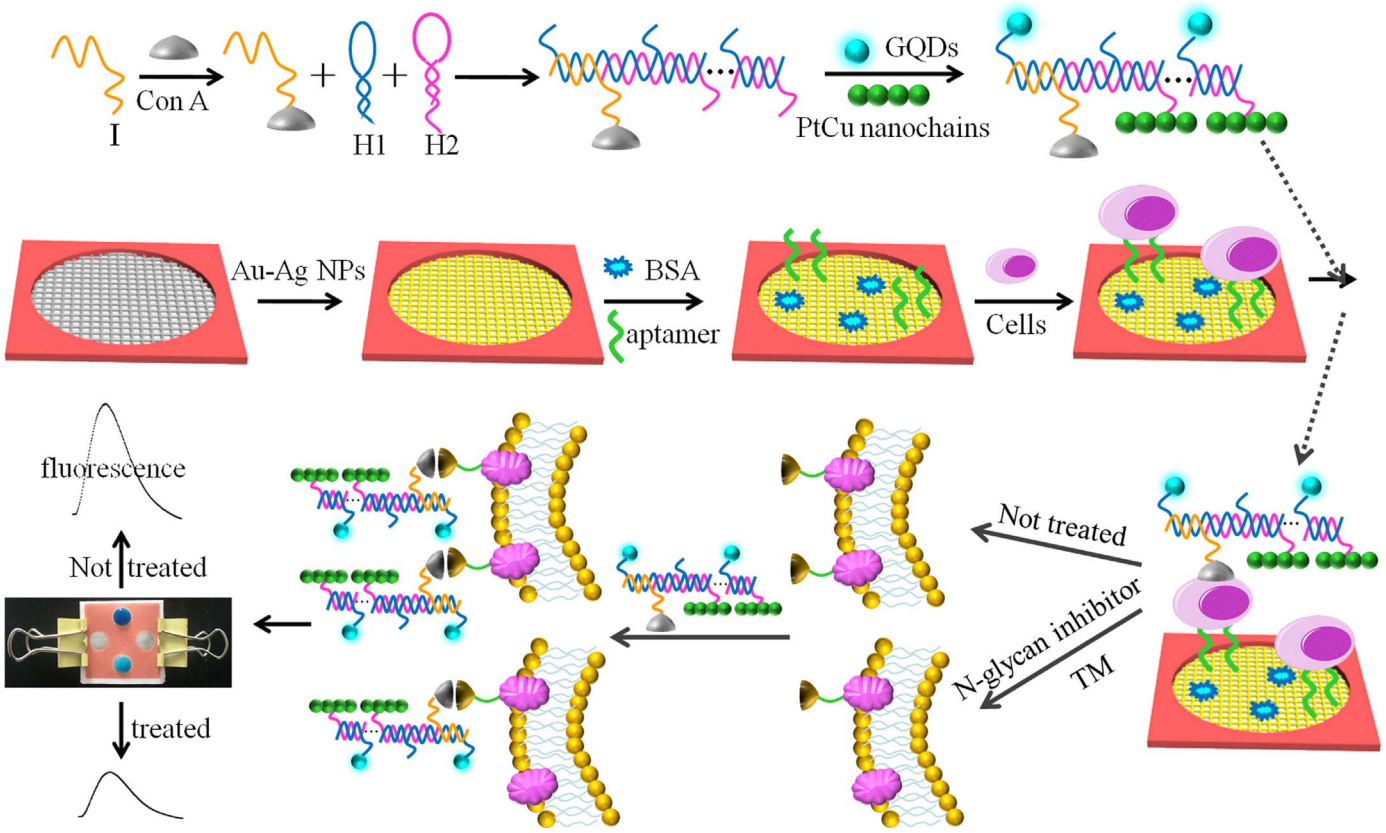


**Scheme 1.** Schematic illustration of the colorimetric/fluorescence bimodal Biosensor for dynamic evaluation of cell surface N-glycan expression.

spectrofluorometer (P.E. USA). Then, two papers were clamped to make them stacked closely (Scheme S1B). After that, 10 μL of 20 mM 3,3̀,5,5̀-tetramethylbenzidine (TMB) was added to paper zone on β-sheet. Subsequently, 5 μL of 2% $H_2O_2$ and 10 μL of 0.2 mM HAc-NaAc buffer (pH 4.0) were added to each paper zone and incubated for 20 min at 30 °C and kept in an ice-water bath for 10 min to terminate the reaction. Finally, a fast color change occurred, thus generating colorimetric signals that could be distinguished by naked eyes or detected through absorbance at 652 nm.

## 3. Results and discussion

### 3.1. Characterization of the modified papers

Ag-Au-μPADs not only increased the surface areas and active sites to immobilize larger amount of aptamers but also effectively reduced the paper background fluorescence (Fig. S5). Their characterization was as follows. The morphologies of the modified paper were characterized by scanning electron microscopy (SEM). As shown in Fig. 1A, the porous bare cellulose paper with smooth microfibers could offer an excellent adsorption microenvironment for the AuNP seeds because of its high ratio of surface area to weight. The SEM image of Fig. 1B,C displayed a type of Au nanorod morphology, a continuous and dense Au nanorod layer was bound on the cellulose fiber surfaces. The successful immobilization of Au nanorod on cellulose fibers was further confirmed by energy dispersive X-ray spectroscopy (EDS) (inset in Fig. 1C) and the peaks of C and Au were observed. As shown in Fig. 1D,E, an Au nanorod and porous Ag bimetallic layer on the cellulose fiber surfaces was observed. The elemental compositions of Ag-Au-μPADs were analyzed with EDS (inset in Fig. 1E) and the EDS analyses showed that the sample consisted of C, Au and Ag elements. The prepared Ag-Au-μPADs still maintained good porous structure, which would benefit the further aptamer modification and analytical application. In order to confirm the crystal structures and to determine the size of particles formed, XRD analysis of the samples was performed. Fig. 1F (lower) showed that one representative diffraction peak appeared at 22.2°, which was corresponding to the cellulose (002) plane (JCPDS 03-0289). the bimetallic Au-Ag NPs were shown in Fig. 1F (upper), which was characterized by another four reflections positioned at $2\theta = 38.3°$, 44.6°, 64.7°, and 77.6° due to the (111), (200), (220), and (311) lattice planes, indicating the successful fabrication of Ag-Au-μPADs (Zhou et al., 2006; Wang et al., 2005).

### 3.2. Characterization of PtCu Nanochains, GQDs and mHCR

The characterization of the as-prepared GQDs were showed in Figs. S6 and S7. The morphology of the as-synthesized PtCu nanochains was characterized by transmission electron microscopy (TEM). In Fig. 2A, it could be seen that the synthesized PtCu product consists of chained nanoparticles with sizes of about 5 nm. These particles were grown in close contact with each other, which formed branched nanochains with a length of hundreds of nanometers. The EDS results showed that the atomic percentage of Pt is about 50% ($Pt_{50}Cu_{50}$, see Fig. 2C). As shown in Fig. 2B, the X-ray diffraction (XRD) patterns showed a fcc structure with peak positions intermediate between Cu and Pt. According to Vegard's law, the peak shifts indicated that the crystal structures were the substitution solid solution of $Pt_{50}Cu_{50}$ with lattice constants of 3.76, 3.85, and 3.89 Å. PtCu nanochains could catalyze the oxidation of TMB by $H_2O_2$ to produce the typical blue color reaction. As shown in Fig. 2D, the maximum absorbance of the reaction mixture at 652 and 370 nm, which originated from the oxidation of

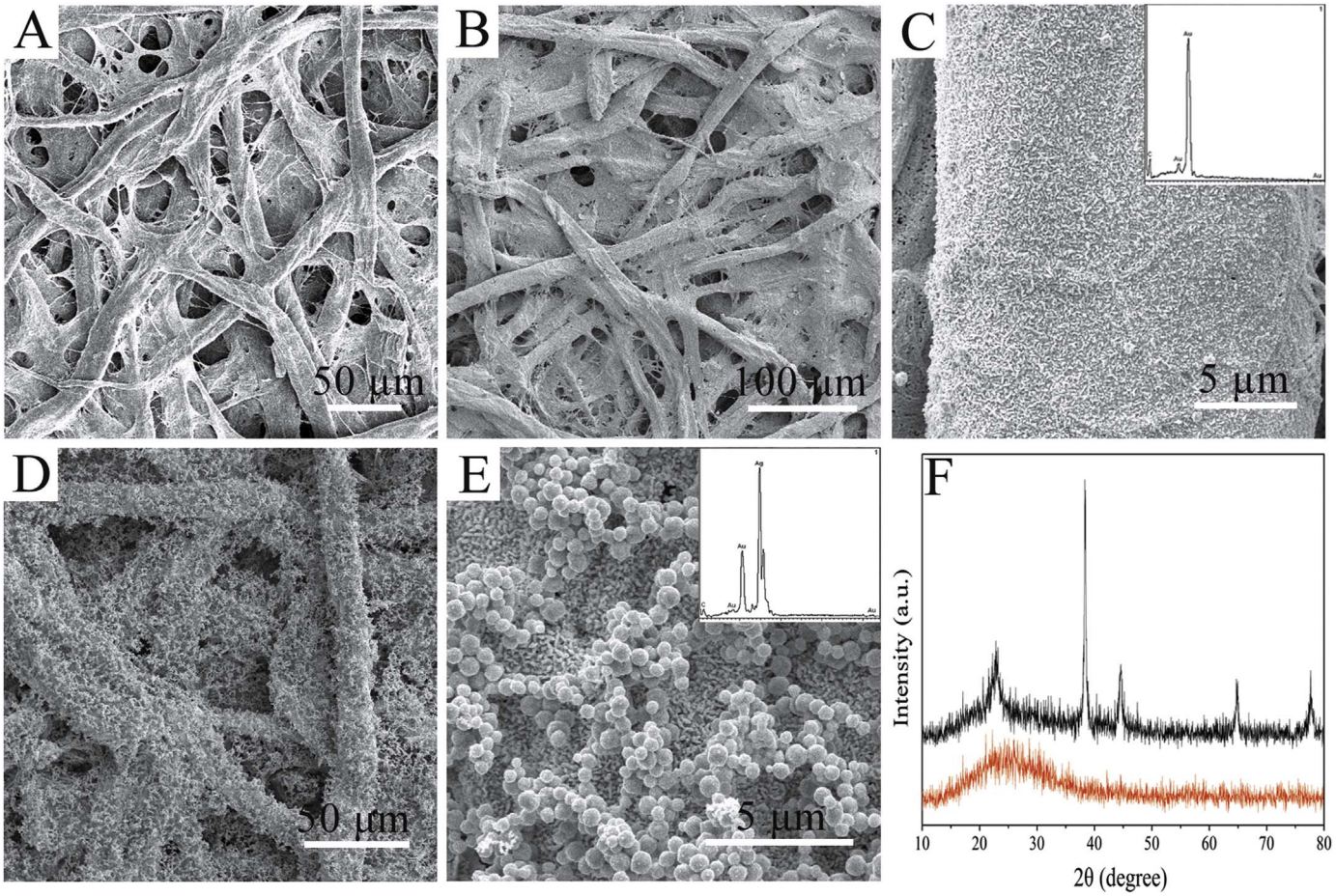


**Fig. 1.** SEM images of (A) pure paperfibers, (B,C) Enlarged Au nanorod layer in paper working zone under different magnification, the inset is EDS image. (D,E) Enlarged Ag-Au bimetallic layer in paper working zone under different magnification, the inset is EDS image; (F) XRD patterns of the μPADs (lower); Ag-Au-μPADs (upper).

TMB. In contrast, no obvious reaction occurred in the absence of PtCu nanochains. The results confirmed that PtCu nanochains exhibit an intrinsic peroxidase-like activity.

To further improve the sensitivity, we employed mHCR to produce long products (over 1500 base pairs, Fig. 3A) with multiple binding sites of GQDs and PtCu nanochains to amplify the signal and multiple branched arms to realize the multivalent binding on the surface. The multivalent binding of HCR products were analyzed using polyacrylamide gel electrophoresis. As shown in Fig. 3A, compared to any one of its constituent domains, the mHCR had less mobility as a result of its collective increased molecular weight, which corresponds to previous reports (Ding et al., 2014; Wu et al., 2013). This confirmed the successful hybridization of the probes.

### 3.3. Cell viability

A nanostructured probe and the modified μPADs should not interfere with the metabolism of the living system for practical biomedical applications. Therefore, in order to inspect the cytotoxicity of the PtCu-mHCR-GQDs bioprobe and the Ag-Au-μPADs, a standard staining method was adapted by the use of the calcein-AM (a living cell dyes) and propidium iodide (PI, a dead cell dyes). Under the fluorescent microscope, green fluorescence in living cells and red fluorescence in dead cells could be observed in cytoplasm of MCF-7 cancer cells (Evenou et al., 2012). Firstly, the cytotoxicity test of the PtCu-mHCR-GQDs bioprobe was performed, two copies of the same MCF-7 cancer cells were respectively incubated with or without the PtCu-mHCR-GQDs bioprobe for 8 h. Media in the dishes were discarded and the cells were gently rinsed twice with PBS. 1 mL of the calcein-AM and PI solution were respectively added into the two dishes and incubated for 15 min at 37 °C. It should be noted that, compared with Fig. 3B, C showed that the percentage of Calcein AM-positive cells and PI-positive cells had not obvious change, which implied that the PtCu-mHCR-GQDs bioprobe had no apparent effect on cancer cells. Next, the cytotoxicity of Ag-Au-μPADs was also studied, MCF-7 cancer cells were incubated with Ag-Au-μPADs. After 4 h of incubation, the cells were stained for 15 min at 37 °C by adding 50 μL of the calcein-AM. As shown in Fig. 3D, MCF-7 cancer cells showed a good living morphology. It should be noted that, Ag-Au-μPADs had no apparent effect on cancer cells. Above all, these results suggested that the as-prepared materials had no apparent harm to cells.

### 3.4. Detection principle for colorimetric/fluorescence behaviors

A mechanism of this biosensor was shown in Scheme 1. Au-Ag-paper devices possessed the large surface areas, which immobilized larger amount of aptamers, then specifically and efficiently captured more cancer cells. The mHCR could produce modified long products with multiple branched arms. It could attach abundant PtCu nanochains and GQDs. Con A was chosen as a recognition element to functionalize the mHCR, Con A could effectively target tumor cells. The binding GQDs on the tumor cells were transformed into fluorescence signal. On the basis of the peroxides-like activity, selective binding PtCu nanochains on the tumor cells can convert the recognition process into quantitative colorimetric signal.

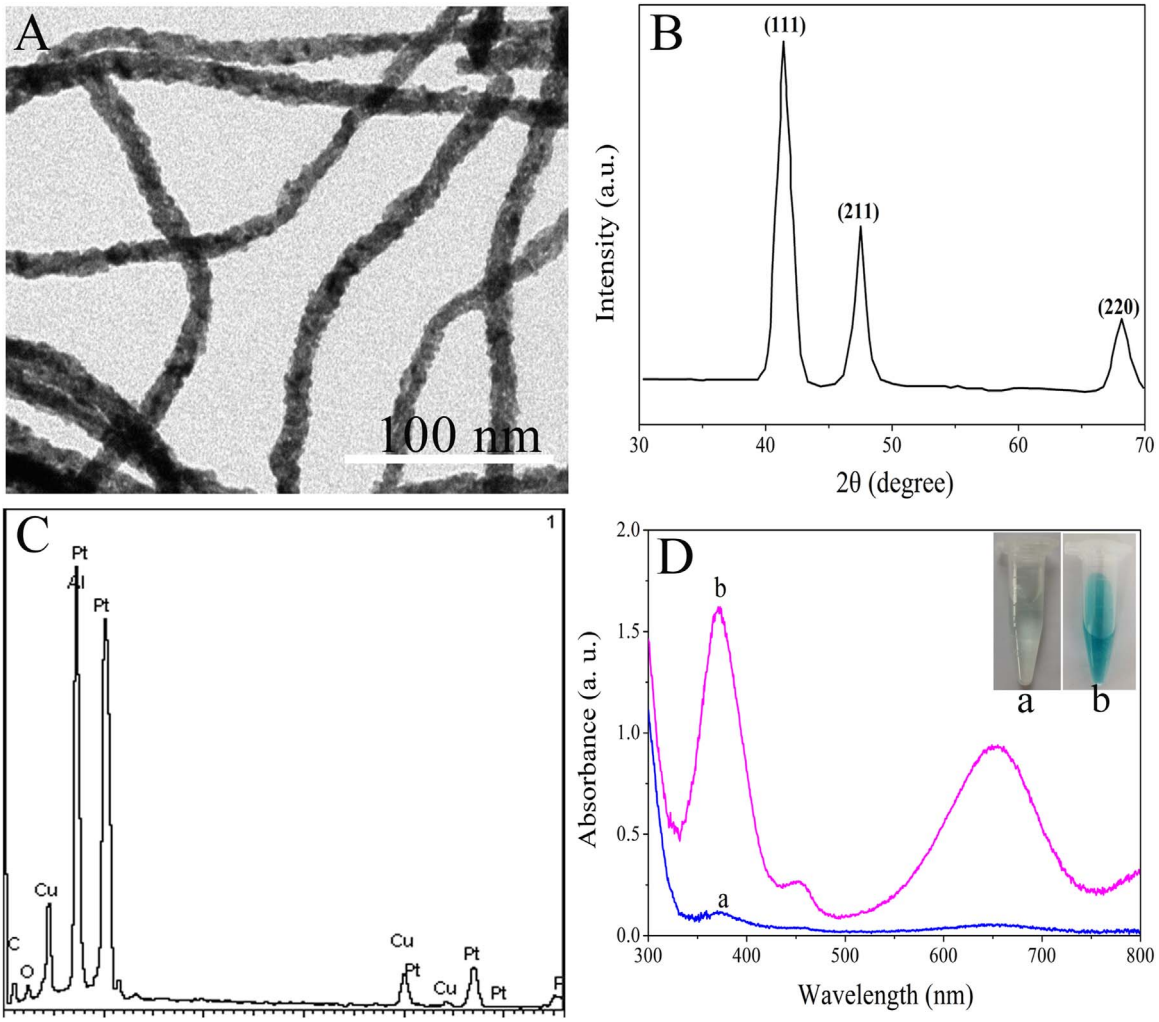


**Fig. 2.** (A) TEM image of the PtCu nanochains with average diameter of about 5 nm; (B) typical XRD patterns and (C) EDS spectrum taken from sample acidified for 4 h; (D) UV–vis spectra of the reaction solution containing 20 mM TMB, 2% $H_2O_2$. (a) In the absence of PtCu nanochains, (b) in the presence of PtCu nanochains. Inset: photographs of different solutions corresponding to parts a and b.

### 3.5. Cytosensing and sensitivity of the biosensor

On the basis of the optimal conditions, the proposed biosensor could be used for cytosensing MCF-7 cells because of the outstanding binding affinity and sensitivity of the MCF-7/BSA/aptamer/Ag-Au-μPADs and PtCu-mHCR-GQDs bioprobe. Firstly, on the α-sheet, the dynamic range for detecting MCF-7 cells with the fluorescence method was also examined (Fig. S9). Next, on the β-sheet, we attempted to detect cancer cells through a colorimetric method. In the presence of TMB and $H_2O_2$, Fig. 4A displayed that the gray intensity increased with the concentration increasing of MCF-7 cells. The gray intensity are proportional to the logarithmic value of the cell concentration ranging from 100 to $1.0\times10^7$ cells $mL^{-1}$. The linear regression equation is $I=18.4\times\log C_{cell}$ (cells $mL^{-1}$) $-5.0$ with the correlation coefficient of $R=0.997$ ($n=5$), where I is the gray intensity and $C_{cell}$ is the MCF-7 cells concentration. The detection limit for cell concentration was estimated to be 33 cells $mL^{-1}$ at $3\sigma$. The proposed biosensor in this work showed a better performance than the previously reported cyto-sensors (Table S1), especially the detection limit.

In order to explain the enhanced sensitivity of the multi-branched hybridization chain strategy, the product of traditional HCR modified by PtCu nanochains and GQD served as the control was compared with the PtCu-mHCR-GQDs bioprobe.

Firstly, the specific binding between Con A and cell surface N-glycan and the signal amplification of the PtCu-mHCR-GQDs bioprobe were studied by colorimetric method. As shown in Fig. 4B, the gray intensity of control was obviously lower than that of the PtCu-mHCR-GQDs. The results showed that the enhanced sensitivity comes from the signal amplification of the PtCu-mHCR-GQDs bioprobe. To further prove the signal amplification effect of the PtCu-mHCR-GQDs, it also could be proved by fluorescence method. The PtCu-mHCR-GQDs provided strong fluorescence in Fig. 4C (mHCR amplification), which suggested that the probes could effectively bind cell surface N-glycan. While Fig. 4C (without amplification) showed much lower fluorescence intensity of the control than that of the PtCu-mHCR-GQDs after the same exposure time.

From the above, it demonstrated that the proposed biosensor exhibited high sensitivity, which could be ascribed to the signal amplification of the mHCR.

### 3.6. N-Glycan expression on MCF-7 cell surface

The dynamic analysis of cell surface N-glycans has primarily significant roles in clinical diagnostics, and it is still vital to uncover their expression and myriad functions perturbed by inhibitors. Under external stimulus, the proposed biosensor allowed it to be further employed for evaluating the dynamic alteration of MCF-7 cells ($10^6$ cells $mL^{-1}$) surface carbohydrate expression with

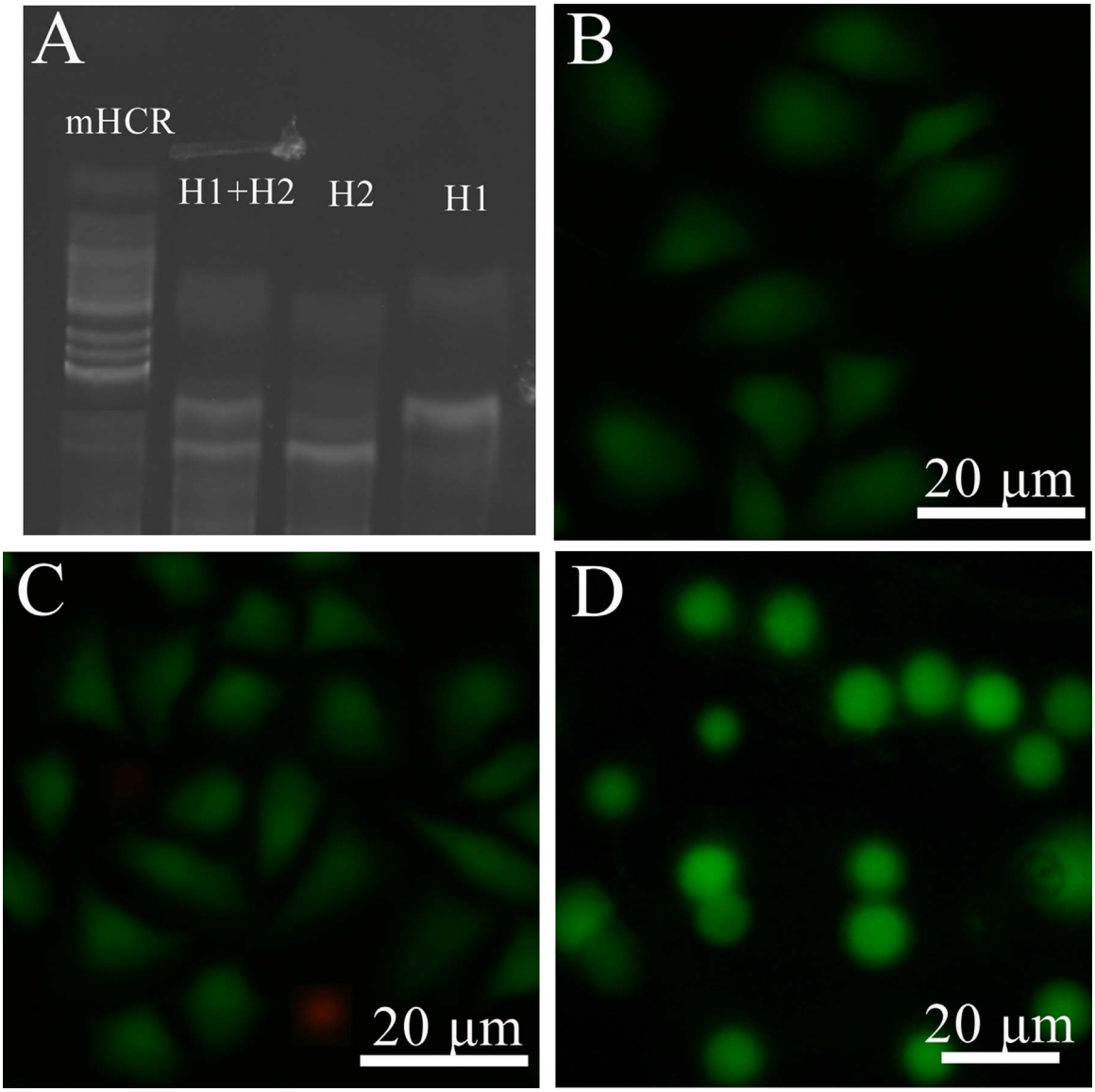


**Fig. 3.** (A) Electrophoretic analysis of the mHCR: lines 1-4 stand for the electrophoretic image of sequences (mHCR, H1+H2, H2 and H1) acquired by annealing. The fluorescence microscopy image of MCF-7 cells (B) before and (C) after treated with the modified HCR-Con A bioprobe. (D) the cytotoxicity of Ag-Au-μPADs.

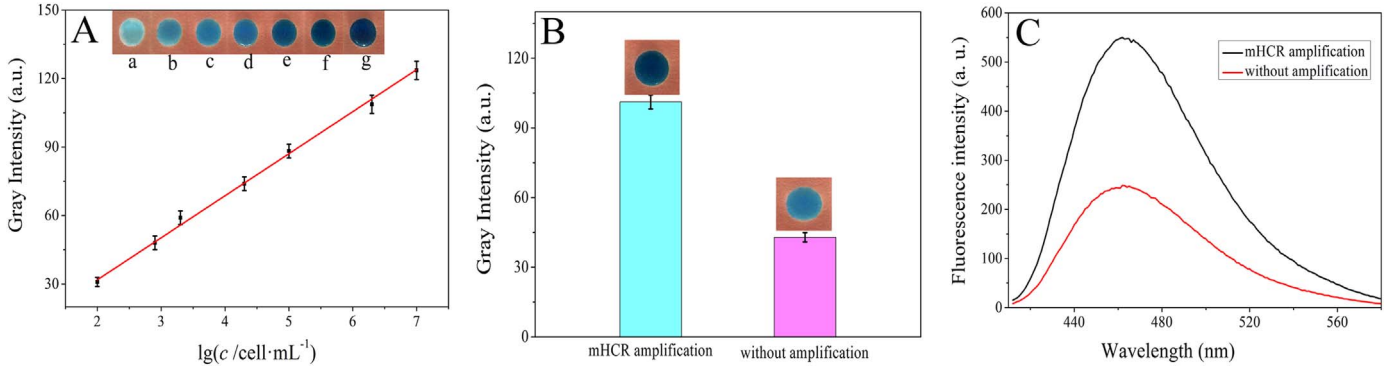


**Fig. 4.** (A) Colorimetric response of MCF-7 cells at the concentrations of 100, 800, $2 \times 10^3$, $2 \times 10^4$, $10^5$, $2 \times 10^6$ and $10^7$ cells $mL^{-1}$, from a-g and calibration curve plotted on a logarithmic scale. Expression of MCF-7 cells without amplification and with mHCR amplification by (B) colorimetric and (C) fluorescence method.

the colorimetric biosensor. Primarily, the inhibitors tunicamycin (TM) was chosen in this work, which could inhibit cell surface N-glycan expression by blocking the first step in the biosynthesis of N-glycosylation in cells (Elbein, 1987). Compared the TM-treated cells with untreated cells, a progressively decreasing gray intensity could be observed in Fig. 5A. After the treatment with TM for 48 h, the cells exhibited weaker gray intensity than those without treatment, and the change in gray intensity was calculated to be 50.5%. The decreased color response of cell surface N-glycan expression was caused by TM. The multi-glycan

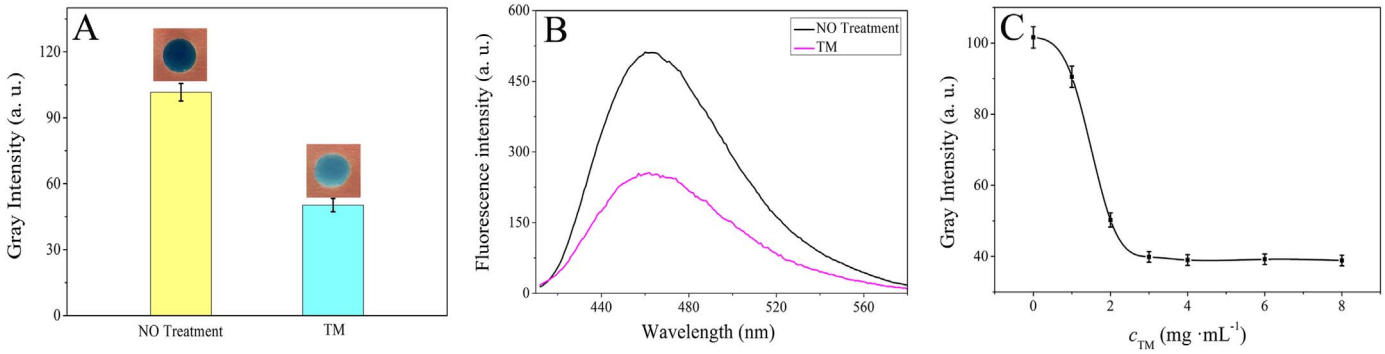


**Fig. 5.** N-Glycan expression of MCF-7 cells surface without or with treatment with TM (2 mg mL$^{-1}$) by (A) colorimetric and (B) fluorescence method. (C) N-Glycan expression of the MCF-7 cells surface after incubation with different concentrations of TM for 48 h. The MCF-7 cells concentration is $1.0 \times 10^6$ cells mL$^{-1}$.

expression of MCF-7 cells was further validated by the fluorescence method. The fluorescent intensity was correlated with the loading extent of the PtCu-mHCR-GQDs on MCF-7 cells, which depended on the binding site numbers on cells, and thus illustrated the amount of target glycan expression. The results were shown in Fig. 5B, after 48 h of treatment with TM, the fluorescence signal change was 49.9%, which confirmed the observed change.

Therefore, the proposed biosensor was able to be applied to dynamically evaluate cell surface N-glycan expression with high sensitivity. Moreover, the inhibition of cell surface N-glycan expression was also evaluated in the presence of different concentrations of TM. As shown in Fig. 5C. It was obvious that the gray intensity decreased with the concentration increasing of TM and gradually reached a steady value after TM concentration was beyond ca. 3 μg mL$^{-1}$. Using these results, the half-maximal inhibition value ($IC_{50}$) was calculated to be 1.6 μg mL$^{-1}$, which was obtained on the basis of the concentration of the half peak gray intensity from the steady gray intensity to the maximal peak gray intensity in the absence of inhibitor. It was similar to that reported with a conventional assay (Matherly et al., 1994). As a result, the proposed biosensor also provided a valuable tool, which had the potential to quantitative screening of small molecule inhibitors of the cell surface N-glycan expression.

### 3.7. *Reproducibility, stability and specificity of the N-glycan-sensor*

The selectivity was investigated to evaluate the feasibility of the proposed method for biological samples, and different cell lines such as K562, A549, and D231 cells were used as the control. As displayed in Fig. S10A, at the same concentration ($1.0 \times 10^6$ cells mL$^{-1}$), the gray intensity of the biosensor negligibly changed with the addition of the control cells, while a significant gray intensity increase was observed for MCF-7 cells. These results demonstrated that the designed biosensor possessed the excellent selectivity due to specificity recognition of MCF-7 cell-targeting aptamer, and it was promising in cancer cell detection and studies of the histopathological lesion process. At a concentration of $1.0 \times 10^6$ cells mL$^{-1}$, the proposed method showed relative standard deviations were less than 5.0% for colorimetric detection and 3.5% for fluorescence detection at three replicate measurements, respectively. The precision and reproducibility of the proposed method were acceptable. In addition, another key factor to be investigated was the stability (Fig. S10B), when the probe was stored at 4 °C, the analytical performance did not decline obviously, showing a good stability. The stability was attributed to the stable structure of bioprobes. Thus, the as-proposed biosensor exhibited good performance in detecting cancer cell with a broad detection range, a low detection limit and reproducibility, which was promising for cancer cell detection and carbohydrate expression evaluation of living cells.

## 4. Conclusions

In conclusion, a novel cytosensing and cell surface N-glycan evaluation could be simultaneously realized with high sensitivity and excellent selectivity based on Au-Ag-μPADs as a platform and the PtCu-mHCR-GQDs as signal labels. In addition, with rational redesign, the mHCR was employed to produce long products with multiple branched arms for multiple PtCu nanochains and GQDs binding, which led to dual signal amplification for highly sensitive detection. Above all, materials involved in our experiments had no apparent influence on the cell viability. Thus, the strategy was successfully used to dynamically analyze changes of cell surface N-glycan in response to inhibitors. It would contribute to the understanding of complex native glycan-related biological processes as well as serve as an impetus for elucidating the physiological processes of N-glycan-related diseases and clinical diagnostics.

## Acknowledgments

This work was financially supported by Special Fund for Shandong Independent Innovation and Achievements Transformation (No. 2014ZZCX02703), the National Natural Science Foundation of China (21575051) and the Natural Science Foundation of Shandong Province, China (ZR2015JL006).

## Appendix A. Supporting information

Supplementary data associated with this article can be found in the online version at http://dx.doi.org/10.1016/j.bios.2016.07.078.

## References

Arnold, J.N., Saldova, R., Galligan, M.C., Murphy, T.B., Mimura-Kimura, Y., Telford, J. E., Godwin, A.K., Rudd, P.M., 2011. J. Proteome Res. 10, 1755–1764.
Bagalkot, V., Farokhzad, O.C., Langer, R., Jon, S., 2006. Angew. Chem. Int. Ed. 45, 8149–8152.
Cao, X., Wang, N., Jia, S., Shao, Y.H., 2013. Anal. Chem. 85, 5040–5046.
Carneiro, M.G., Koharudin, L.M.I., Ban, D., Sabo, T.M., Trigo-Mourino, P., Mazur, A., Griesinger, C., Gronenborn, A.M., Lee, D., 2015. Angew. Chem. Int. Ed. 54, 6462–6465.
Choi, H.M.T., Chang, J.Y., Trinh, L.A., Padilla, J.E., Fraser, S.E., Pierce, N.A., 2010. Nat. Biotechnol. 28, 1208–1212.
Dennis, J.W., Nabi, I.R., Demetriou, M., 2009. Cell 139, 1229–1241.
Deiss, F., Funes-Huacca, M.E., Bal, J., Tjhung, K.F., Derda, R., 2014. Lab Chip 14, 167–171.
Deiss, F., Mazzeo, A., Hong, E., Ingber, D.E., Derda, R., Whitesides, G.M., 2013. Anal. Chem. 85, 8085–8094.
Ding, Y., Wang, Y., Zhang, L.C., Zhang, H., Lei, Y., 2012. J. Mater. Chem. 22, 980–986.
Ding, Y., Liu, X., Zhu, J., Wang, L., Jiang, W., 2014. Talanta 125, 393–399.
Dirks, R.M., Pierce, N.A., 2004. Proc. Natl. Acad. Sci. USA 101, 15275–15278.
Elbein, A.D., 1987. Annu. Rev. Biochem. 56, 497–534.

Evenou, F., Meglio, J.M.D., Ladoux, B., Hersen, P., 2012. Lab Chip 12, 1717–1722.
Ge, L., Yan, J.X., Song, X.R., Yan, M., Ge, S.G., Yu, J.H., 2012. Biomaterials 33, 1024–1031.
Ge, S.G., Liu, F., Liu, W.Y., Yan, M., Song, X.R., Yu, J.H., 2014. Chem. Commun. 50, 475–477.
Gosso, S., Gavello, D., Giachello, C.N.G., Franchino, C., Carbone, E., Carabelli, V., 2011. Biomaterials 32, 9040–9050.
Gu, J.G., Isaji, T., Xu, Q.S., Kariya, Y., Gu, W., Fukuda, T., Du, Y.G., 2012. Glycoconj. J. 29, 599–607.
Huang, J., Wu, Y.R., Chen, Y., Zhu, Z., Yang, X.H., Yang, C.J., Wang, K.M., Tan, W.H., 2011. Angew. Chem. Int. Ed. 50, 401–404.
Kovarik, M.L., Gach, P.C., Ornoff, D.M., Wang, Y., Balowski, J., Farrag, L., Allbritton, N. L., 2012. Anal. Chem. 84, 516–540.
Lan, F.F., Sun, G.Q., Liang, L.L., Ge, S.G., Yan, M., Yu, J.H., 2016. Biosens. Bioelectron. 79, 416–422.
Loh, K.P., Bao, Q., Eda, G., Chhowalla, M., 2010. Nat. Chem 2, 1015–1024.
Liang, L.L., Lan, F.F., Li, L., Su, M., Ge, S.G., Yua, J.H., Liu, H.Y., Yan, M., 2016. Biosens. Bioelectron. 82, 204–211.
Li, C.Z., Vandenberg, K., Prabhulkar, S., Zhu, X., Schneper, L., Methee, K., Rosser, C.J., lmeide, E., 2011. Biosens. Bioelectron. 26, 4342–4348.
Li, W.P., Li, L., Li, M., Yu, Y.H., Ge, S.G., Yan, M., Song, X.R., 2013. Chem. Commun. 49, 9540–9542.
Matherly, L.H., Angeles, S.M., 1994. Biochem. Pharmacol. 47, 1094–1098.
Meyvantsson, I., Beebe, D.J., 2008. Annu. Rev. Anal. Chem. 1, 423–449.
Nishikaze, T., Kaneshiro, K., Kawabata, S., Tanaka, K., 2012. Anal. Chem. 84, 9453–9461.
Park, S., Jeong, R.A., Boo, H., Park, J., Kim, H.C., Chung, T.D., 2012. Biosens. Bioelectron. 31, 284–291.
Pilobello, K.T., Mahal, L.K., 2007. Curr. Opin. Chem. Biol. 11, 300–305.
Primack, J., Flynn, G.C., Pan, H., 2011. Electrophoresis 32, 1129–1132.
Ratanatawanate, C., Chyao, A., Balkus, K.J., 2011. J. Am. Chem. Soc. 133, 3492–3497.
Royle, L., Campbell, M.P., Radcliffe, C.M., White, D.M., Harvey, D.J., Abrahams, J.L., Kim, Y.G., Henry, G.W., Shadick, N.A., Weinblatt, M.E., Lee, D.M., Rudd, P.M., Dwek, R.A., 2008. Anal. Biochem. 376, 1–12.
Shangguan, D., Li, Y., Tang, Z., Cao, Z.C., Chen, H.W., Mallikaratchy, P., Sefah, K., Yang, C.J., Tan, W., 2006. Proc. Natl. Acad. Sci. USA 103, 11838–11843.
Vanderschaeghe, D., Szekrényes, A., Wenz, C., Gassmann, M., Naik, N., Bynum, M., Yin, H., Delanghe, J., Guttman, A., Callewaert, N., 2010. Anal. Chem. 82, 7408–7415.
Wang, A.Q., Liu, J.H., Lin, S.D., Lin, T.S., Mou, C.Y., 2005. J. Catal. 233, 186–197.
Wang, X., Lou, X.H., Wang, Y., Guo, Q.C., Fang, Z., Zhong, X.H., Mao, H.J., Jin, Q.H., Wu, L., Zhao, H., Zhao, J.L., 2010. Biosens. Bioelectron. 25, 1934–1940.
Wu, C., Han, D., Chen, T., Peng, L., Zhu, G., You, M., Qiu, L., Sefah, K., Zhang, X., Tan, W., 2013. J. Am. Chem. Soc. 135, 18644–18650.
Wu, P., Li, Y., Yan, X.P., 2009. Anal. Chem. 81, 6252–6257.
Xu, C.X., Liu, Y.Q., Su, F., Liu, A.H., Qiu, H.J., 2011. Biosens. Bioelectron. 27, 160–166.
Yeo, L.Y., Chang, H.C., Chan, P.P.Y., Friend, J.R., 2011. Small 7, 12–48.
Zhou, M., Chen, S.H., Zhao, S.Y., Ma, H.Y., 2006. Physica E 33, 28–34.
Zhu, S.J., Zhang, J.H., Qiao, C.Y., Tang, S.J., Li, Y.F., Yuan, W.J., Li, B., Tian, L., Liu, F., Hu, R., Gao, H.N., Wei, H.T., Zhang, H., Sun, H.C., Yang, B., 2011. Chem. Commun. 47, 6858–6860.